Segmentation and Artifact Removal in Microwave-Induced Thermoacoustic Imaging

Hao Nan, *Student Member*, *IEEE*, Tzu-Chieh Chou, *Student Member*, *IEEE*, and Amin Arbabian, *Member*, *IEEE*

***Abstract*— Microwave-induced thermoacoustic (TA) imaging combines the soft-tissue dielectric contrast of microwave excitation with the resolution of ultrasound for the goal of a safe, high resolution, and possibly portable imaging technique. However, the hybrid nature of this method introduces new image-reconstruction challenges in enabling sufficient accuracy and segmentation. In this paper, we propose a segmentation technique based on the polarity characteristic of TA signals. A wavelet analysis based method is proposed to identify reflection artifacts as well. The time-frequency feature of the signal is used to assist differentiating artifacts. Ex vivo verification with experimental data is also provided.**

I. Introduction

A medical imaging technology capable of sufficient soft-tissue contrast while providing a hand-held form factor has been a goal of biomedical engineering. Potential applications include identification of abnormal tissue (e.g., in widespread cancer screening), early and on-site detection of internal injuries and hemorrhages, and other ambulatory care situations that need immediate and on-site access. Microwave-induced thermoacoustic (TA) imaging [1-3] combines the soft-tissue contrast of microwave excitation with the resolution of ultrasound detection, while posing no ionizing radiation, and could enable a portable imaging device for these goals.

In the TA technique, the target absorbs part of the energy of the incident electromagnetic pulse based on the specific microwave absorption properties, inducing an increase in temperature on the order of millikelvins. Due to this sudden thermal expansion, an acoustic stress wave in the ultrasonic range is generated from the internal boundaries of the target structure. This stress wave contains information on microwave absorption and the thermal and structural properties of the tissue. It is detected by the ultrasonic transducer or a transducer array. The microwave-induced TA technique combines the advantages of microwave and ultrasound imaging, namely penetration depth, contrast, and high resolution [1].

After the initial capture and reconstruction of the image, further processing for image segmentation and artifact removal is the first step toward automatic analysis and evaluation. Accurate segmentation and detection of tissue boundaries is critical for clinical diagnosis and decision-making, but it has not been completely addressed for TA imaging. One of the conventional segmentation approaches is the intensity-gradient technique [4]. Considering the bipolar nature of TA signal, this method cannot be readily applied. We propose a polarity gradient method for segmentation of TA imaging.

To further suppress image artifacts (e.g., due to secondary reflections), we rely on the differences in the frequency spectrum of the artifacts compared to actual target response, and use the time-frequency characteristics of the image data to identify and remove these errors. We use the Morlet wavelet transform to analyze the time-frequency characteristics of the signal. After the elimination of noise and artifacts segmentation, the proposed algorithm finds the edge of the tissue and relative microwave absorption rate of different tissue materials.

II. Methods

A. Operation Principle

The generation of the TA signal follows the equation [5]

$$(\nabla^2 - \frac{1}{v_s^2}\frac{\partial^2}{\partial t^2})\, p(r,t) = -\frac{\beta}{C}\frac{\partial H(r,t)}{\partial t}.$$

Here, $p(r,t)$ is the stress at position r and time t, v_s is the speed of sound, β is the thermal expansion coefficient, C is the specific heat capacity, and $H(r,t)$ is the heating function, defined as thermal energy absorbed per unit time and unit mass. The term on the right-hand side of the equation is the time derivative of the energy deposition. The sharp slopes at the rising and falling edges of a square pulse lead to efficient stress wave generation. Consequently, the generated stress wave is a bipolar signal whose peak and valley correspond to the sequential expansion and contraction of the tissue, as shown in Fig. 1.

The primary contrast in TA imaging comes from the differences in electromagnetic energy absorption, due to variations in dielectric properties. For example, higher effective conductivity leads to a larger absorption in the microwave spectrum. Unlike MRI or X-Ray imaging, the direct application of this technique only maps the *boundaries* between different tissue types and does not give a direct reconstruction of the internal composition. As a result, it is critical to correctly identify the boundaries, and then, it will be important to develop an indirect way of identifying and mapping tissue characteristics in between these boundaries.

Fig. 1 shows a typical measured TA signal. It displays two bipolar components with opposite polarities, indicated by the arrows in Fig. 1(a). These two signals are from the top and bottom surfaces of the tissue sample, which is placed in mineral oil. The sample has a higher microwave absorption

Research supported by Center of Integrated Systems, Stanford University.

Hao Nan and Amin Arbabian are with the Department of Electrical Engineering at Stanford University, Stanford, CA 94305 USA. (corresponding author is Hao Nan: e-mail: haonan@stanford.edu).

Tzu-Chieh Chou is with the Department of Electrical Engineering at National Taiwan University, Taipei, 10617 Taiwan.

rate, therefore, it absorbs the electromagnetic energy and expands in the direction of the surrounding material (oil), as shown in Fig. 1(b). The generated stress waves from each of the boundaries propagate upwards and downwards. The upward-propagating signals are picked up by the transducer. Due to polarity of transducer, a displacement in z direction leads to a negative voltage. Consequently the received bipolar signals coming from the two boundaries have opposite polarities. This relative phase information will be used for target differentiation and identification. Zero-crossings of this signal will be used to map the structural boundaries.

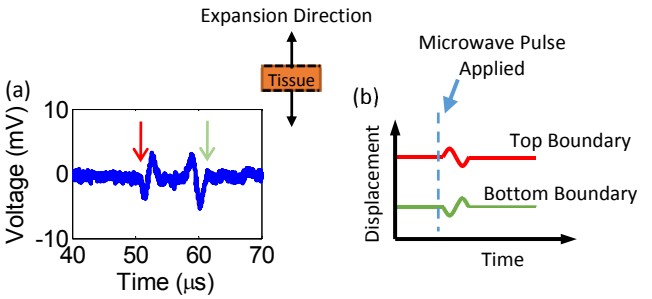

Figure. 1. (a) An example measured TA signal. The x-axis is the time after the microwave excitation pulse. The y-axis is the measured signal voltage. The imaging sample is a piece of chicken breast with the thickness of approximately *11mm*. The black arrows in the target indicate the expansion direction of the boundaries after the microwave excitation. (b) The displacement of the top (red) and bottom (green) boundaries after the application of microwave pulse.

B. *Experiment Setup*

We run an ex vivo experiment to capture the data for segmentation processing. A tissue sample is placed in a container filled with mineral oil. A signal generator produces a square pulse-modulated sine wave with a carrier frequency of 2.1 GHz. A solid-state GaN power amplifier is used to provide a peak power of up to 120 W. Unlike other solutions [1, 2], which employ *kW* sources, our approach focuses on a low power solid-state solution to enable future integration with a hand-held device. A waveguide couples the microwave pulse to the container in a non-contact manner. A matching network is employed for impedance matching to enhance power transmission efficiency. Mineral oil has a small microwave absorption coefficient and provides a good acoustic coupling between the tissue and the transducer. Moreover, stress waves experience little attenuation in mineral oil, which simplifies the characterization process. In the receiver path, an immersion piezoelectric transducer with a central frequency of 0.5 MHz is used. A low-noise amplifier (LNA) is employed for conditioning. A linear stage setup is used to perform a B-scan to acquire the image.

We use a modified back-projection algorithm for reconstruction [6]. This algorithm considers the spherical nature of propagation for the TA signal and the effect of transducer beam profile. The algorithm can improve SNR, and is relatively fast in terms of processing. Since the transducer receives signals from all the directions within its beam width, the signal received at a specific time and transducer scan step is the integral of the stress waves from a spherical surface with the weights of transducer beam profile:

$$p_r(r_0,t_0) = \iiint_{|t-t_0|=|r-r_0|/v_s} p(r,t)\cdot B(r,r_0)dr$$

Here, $p_r(r_0,t_0)$ is the signal received by the transducer at position r_0 at time t_0, and $B(r,r_0)$ is the beam profile at position r, if the transducer is at position r_0.

For reconstruction, the measured signal at position r_0 is back projected along a sphere with the weight of the beam profile of the transducer. The signals from different transducer positions are combined to form the reconstructed image. The TA signal will sum coherently while the noise is summed incoherently. As a result, the SNR improves. The speed of sound in tissue is approximately *1.5mm/μs*, which is assumed constant for the back-projection algorithm.

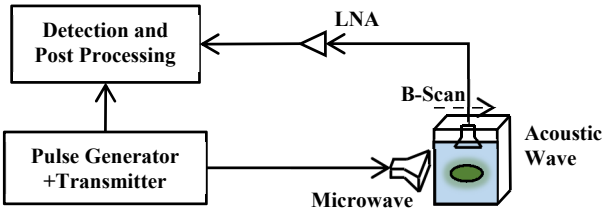

Figure. 2. The schematic diagram of the experiment setup.

C. *Polarity Gradient Method*

After image reconstruction, segmentation is an important step in image analysis. Considering the bipolar nature of the TA signal, we can detect the tissue boundaries by finding the zero-crossing points of the measured TA signal. In our proposed method, we first create a polarity map, defined as *polarity map = sign(original image)*. A +1 value is assigned if the original image pixel is positive and -1 is assigned if it is negative. The TA signal has a high dynamic range, so we only consider its polarity by normalizing its magnitude. The second step is to use an edge detector on the polarity map to identify boundaries. In TA imaging, the polarity of the TA signal is related to the expansion direction of the tissue, and this will be used as a signature to differentiate target properties. For example, muscle expands in the direction of fat because muscle has a higher microwave absorption rate. This polarity, or phase information, helps classify the relative microwave absorption rates of adjacent tissue materials. The gradient of the polarity map has the same direction as the tissue expansion.

However, noise and reflection artifacts also have zero-crossing points that are identified by the edge detector. They need to be identified and distinguished from the real targets. To identify noise zero-crossing points, we run a thresholding function on the spatial average of the absolute values of the image with an averaging size of 3×3 mm. The absolute values are used because the signal is bipolar. Noise has a small average value and is filtered by the threshold. The results form a *signal check map* shown in the next section.

D. *Artifact Removal*

Generated stress waves are reflected at some boundaries, such as tissue boundaries, which produce additional reflection artifacts. These artifacts lose some high frequency components due to reflection, acoustic re-absorption and scattering [7]. Consequently they have different frequency spectrum shape compared to real tissue signals. This fact motivates us to look into the time-frequency information contained in the measured signal. For this purpose, we use the

continuous wavelet transform (CWT) as a natural generalization of the Fourier transform for time-frequency analysis [8]. CWT uses a wavelet function, instead of the complex exponential function of Fourier transform, as the kernel in the integral transform. The operation of scaling wavelet function resembles frequency shifting in short-time Fourier transform (STFT), and the corresponding pseudo-frequency at each scale can be calculated with a known wavelet function. The CWT approach provides flexibility in terms of selecting different wavelets and scales, which makes it a more powerful tool for analyzing acoustic signals compared to STFT, which is limited by a fixed frequency resolution [8]. We use the Morlet wavelet because its waveform is similar to the impulse response of the transducer. The CWT coefficients are normalized to eliminate the energy of the signal and only the frequency spectrum shape is used for differentiation. The real tissue signal has larger components in the high frequency range in the normalized CWT, when compared to the artifacts, which is used as a signature to distinguish between the two. To increase decision accuracy, we segment the A-scan signal into partially overlapped time windows called *frames*, and decide whether each frame contains a real tissue signal or not. In order to reduce variance, the average value of the wavelet coefficients in the frame over time is used to make the decision. We use a frame length of 2μs and a 50% overlap between frames, as a trade-off between temporal resolution and variance reduction. After the wavelet analysis step, the results are combined to form a 2D *tissue check map.* The final segmentation results combine the signal check map and tissue check map to remove the noise and artifact contributions.

III. Results and Discussion

Fig. 3(a) shows the imaging sample used in the experiment. It is a layered muscle-fat-muscle sandwich structure. Fig. 3(b) shows the 2D reconstructed image using the modified back-projection algorithm. Artifacts are observable at a depth greater than 90mm. These artifacts are due to reflections of TA signals at the tissue's internal boundaries. We calculate the polarity map gradient using an edge detector. In Fig. 3(c) we show the gradient of the polarity image. The different colors correspond to different expansion direction. However, some edges are due to noise rather than signal. We check each pixel and decide whether it is signal or noise using the proposed averaging method in section II. The resulting signal check map is shown in Fig. 3(d). The white sections represent regions containing signal, and the black sections contain only noise. Combining Fig. 3(c) and (d), we can find the zero crossing points of the original image and eliminate the contributions of the noise. The results from this part are shown in Fig. 3(e).

Some segmentation results are due to the reflection artifacts and cannot be filtered by the signal check map in Fig. 3(d). In order to suppress these artifacts, for each A-scan signal, we perform a CWT using a Morlet wavelet. The Morlet wavelet transform of the signal in Fig. 4(a) is shown in Fig. 4(b). The signal in Fig. 4(a) is measured above the center of the imaging sample. We normalize CWT results by dividing the maximum value of CWT at each time step. The normalized CWT results are shown in Fig. 4(c).

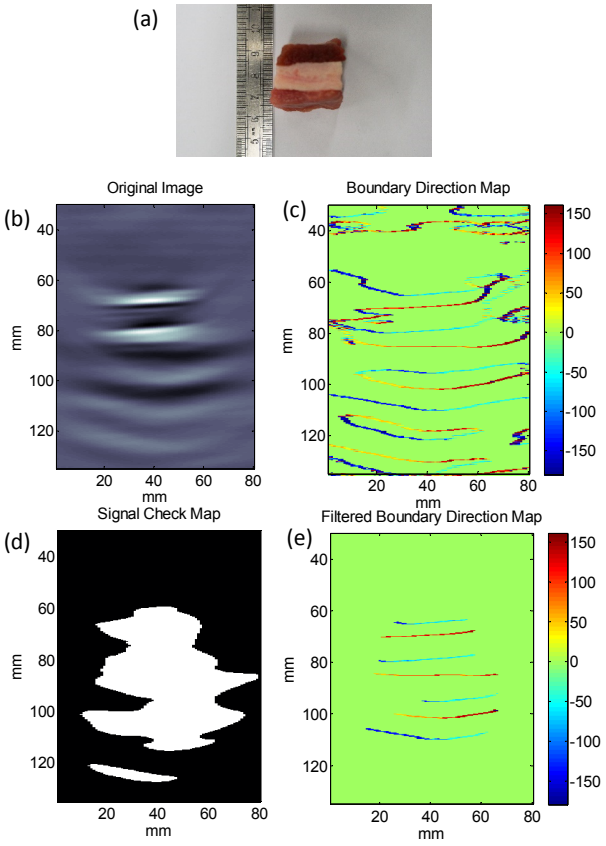

Figure. 3. (a) The muscle-fat-muscle sample used in the experiment. (b) The reconstructed image using the modified back-projection algorithm. (c) The gradient of polarity map. The colorbar shows the angle of the direction in degree. (d) The signal check map, which determines whether the region has signal. (e) Filtered boundaries with direction of the gradient. This step combines the outcomes of (c) and (d).

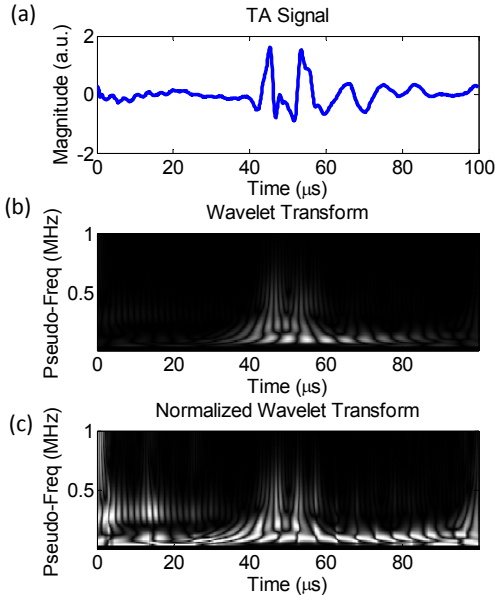

Figure. 4. (a) The measured A-scan signal. (b) CWT of A-scan signal. (c) The normalized CWT. The CWT results are shown in pseudo-frequency.

We divide the A-scan signal into frames with a 2 μs time window. For each frame, we take the wavelet coefficients and calculate the average over time, as shown in Fig. 5(a) for a particular frame. The resulting signal is an averaged wavelet coefficient of that frame. This mean normalized spectrum captures the spectral shape information of each frame, and we use this as a criterion to differentiate the TA signal from the artifacts. In Fig. 5(b), the plot shows that the tissue TA signal has a peak between the pseudo-frequencies 0.2MHz and 0.3MHz, which is larger than the artifact signal's peak. This difference is used to distinguish real tissue signal from artifact signals. By setting an appropriate threshold, we can identify and differentiate imaging artifacts. Fig. 5(c) shows a 2D plot of mean-normalized spectrum of the measured A-scan signal in Fig. 4(a). The white box shows the region of interest for real tissue signals.

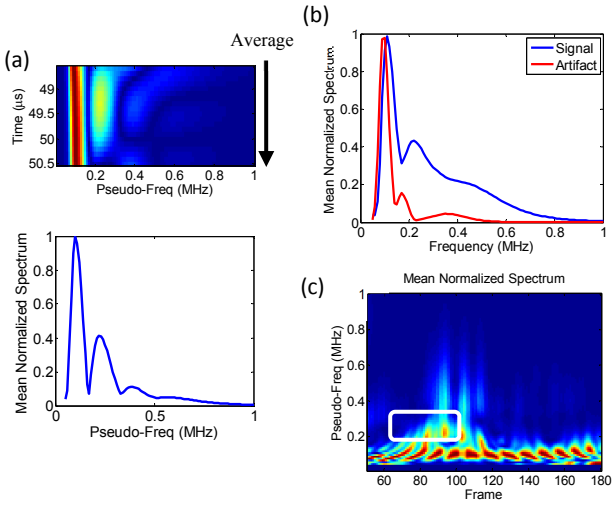

Figure. 5. (a) The wavelet coefficients are averaged over the time to obtain mean normalized spectrum. (b) The comparison of mean normalized spectrum between real tissue signal and artifact. (c) The mean normalized spectrum vs. frame. The white box shows the signature of real tissue signal.

The tissue check map after the wavelet analysis is shown in Fig. 6(a). The white regions indicate that the pixel is a tissue signal and the black regions are noise and artifacts. Fig. 6(b) shows the final segmentation results, which combines Fig. 6(a) and Fig. 3(e) results. Fig. 6(c) shows the final segmentation image. We can see that the boundaries of the muscle and fat parts are successfully found. In general, the cold colors show that the expansion direction is upward and warm color shows that the expansion direction is downward. From this information, we can see that the segmentation result between 63–70mm and 80–90mm have more microwave absorption than the surroundings. The "H" indicates the relative high microwave absorption region and "L" indicates the relative low microwave absorption region. These results are in agreement with the real imaging sample. Our experiment uses a B-scan with single-element transducers, so the vertical boundaries are not shown or detected.

IV. Conclusion

In this paper, we propose a segmentation method for microwave-induced TA imaging. This method utilizes the bipolar nature of the TA signal. Additionally, a wavelet-based method for artifacts identification and removal is proposed. This method is verified by ex vivo experiment data, and the results are consistent with the real imaging sample. Future work includes the application of these techniques to more complex tissue structures.

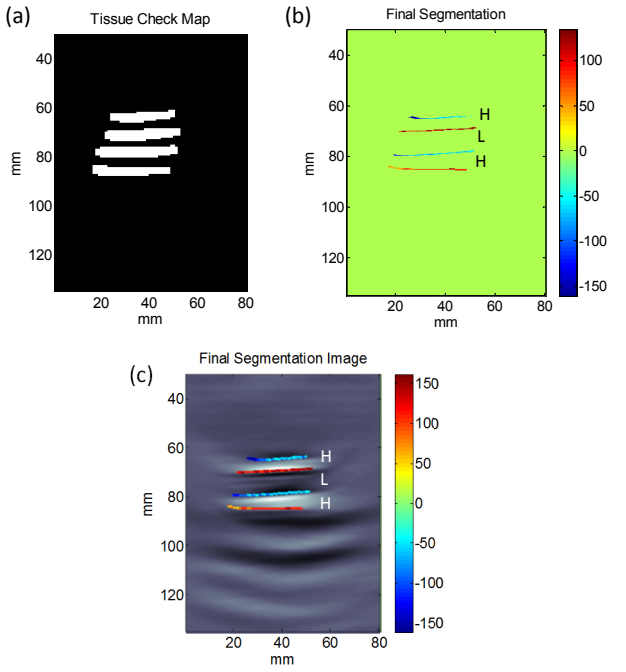

Figure. 6. (a) Tissue check map using wavelet analysis. (b) The final segmentation results which takes the wavelet analysis results into consideration. (c) The final segmentation image showing the actual boundaries. It also shows the expansion direction of the boundaries.

Acknowledgement

The authors thank Rohde & Schwarz for assistance with measurement equipment as well as RFMD, Infineon, TI, and Maxim Integrated for equipment donations. This work was supported in part by the Center for Integrated Systems, Stanford University.

References

[1] G. Ku and L. Wang, "Scanning thermoacoustic tomography in biological tissue," *Medical Physics*, vol. 27, no. 5, pp. 1195–1202, May 2000.

[2] B. Guo, J. Li, H. Zmuda, and M. Sheplak, "Multifrequency microwave-induced thermal acoustic imaging for breast cancer detection," *IEEE Transactions on Bio-Medical Engineering*, vol. 54, no. 11, pp. 2000–2010, Nov. 2007.

[3] M. Omar, S. Kellnberger, G. Sergiadis, D. Razansky, and V. Ntziachristos, "Near-field thermoacoustic imaging with transmission line pulsers," *Medical Physics*, vol. 39, no. 7, pp. 4460–4466, Jul. 2012.

[4] J. Noble and D. Boukerroui, "Ultrasound image segmentation: a survey," *Medical Imaging, IEEE Transactions on*, vol. 25, no. 8, pp. 987–1010, Aug. 2006.

[5] M. W. Sigrist, "Laser generation of acoustic waves in liquids and gases," *Journal of Applied Physics*, vol. 60, no. 7, p. R83, 1986.

[6] M. Xu and L. Wang, "Universal back-projection algorithm for photoacoustic computed tomography," *Physical Review E*, vol. 71, no. 1, p. 016706, Jan. 2005.

[7] S. N. Narouze, *Atlas of Ultrasound-Guided Procedures in Interventional Pain Management.* New York: Springer, 2011, ch. 2.

[8] A.-H. Najmi and J. Sadowsky, "The continuous wavelet transform and variable resolution time-frequency analysis," *Johns Hopkins Apl Technical Digest*, vol. 18, no. 1, pp. 134–140, 1997.